

000
001
002054
055
056

Multi-channel Weighted Nuclear Norm Minimization for Real Color Image Denoising

057
058
059003
004
005
006
007060
061
062
063

Anonymous ICCV submission

008
009
010
011064
065
066

Paper ID 572

012
013
014
015067
068
069

Abstract

The noise structures among the R, G, B channels of real images are quite different due to the preprocessing steps, such as demosaicing, white balance, etc., of the in-camera imaging pipelines. This makes the real image denoising problem much more complex than traditional grayscale image denoising. In this paper, we propose a multi-channel optimization model for real color image denoising. Specifically, we introduce a weighting matrix into the data term to process adaptively each part of R, G, B channels in the joint patches concatenated by corresponding patches in these channels. In the regularization term, we employ the weighted nuclear norm to exploit the non-local self similar property. The proposed multi-channel weighted nuclear norm minimization (WNNM) model is much more complex than the standard WNNM model. We reformulate the proposed model into a linear equality-constrained optimization problem and solve it by the alternating direction method of multipliers algorithm. Each alternative updating step has closed-form solution and the convergence results are given. Experiments on benchmark datasets demonstrate that the proposed model outperforms state-of-the-art denoising methods on synthetic as well as real-world noisy images.

lent denoising performance by exploiting the NSS property via low rank regularization.

The real color image denoising problem is not a trivial extension from single channel (grayscale image) to multiple channels (color image). The reason is that the noise structures are quite different among the Red (R), Green (G), Blue (B) channels of images captured by CCD or CMOS cameras due to the on-board processing steps [13]. This makes the real color image denoising problem much more complex. Directly applying the denoising methods for grayscale images to each channel of color images separately would obtain bad performance [14]. There are several work [14–19] proposed specifically for color image denoising. The method [15] first transforms the color images into the luminance/chrominance space such as YCbCr before denoising, but this would make the noise distribution more complex in color images. The methods of [14, 19] process the joint patches concatenated by the corresponding patches in R, G, B channels and treat equally the patches in different channels. This would generate false colors or artifacts [14]. The methods of [16–18] ignore the non-local self similarity property of natural images, and their performance would be largely depressed [2, 7].

In order to deal with the R, G, B channels in color images more effectively, different noise properties of different channels should be considered in solving real color image denoising problem. Besides, due to its expressive denoising performance, the WNNM model [7] is employed to exploit the NSS property of natural images. In this paper, we proposed a multi-channel WNNM model for real color image denoising. By introducing a weighting matrix to the WNNM model, the proposed multi-channel WNNM model no longer has closed-form solutions and more challenging to solve. By reformulating the proposed multi-channel WNNM model into a linear equality-constrained program with two variables, the relaxed problem can be solved under the alternating direction method of multipliers (ADMM) [20] framework. Each variable can be updated with closed-form solution [7, 21]. We also give the convergency results with detailed proof to guarantee a rational termination of

1. Introduction

Image denoising is an important problem in enhancing the image quality in computer vision systems. The traditional grayscale image denoising problem aims to recover the clean image \mathbf{x} from the noisy observation $\mathbf{y} = \mathbf{x} + \mathbf{n}$, where \mathbf{n} is often assumed to be additive white Gaussian noise (AWGN). Most image denoising methods in this field either employ the non-local self similarity (NSS) of natural images [1–7] or learn generative or discriminative denoisers from paired natural clean images and synthetic noisy images [8–12]. Among these methods, the weighted nuclear norm minimization (WNNM) method achieves exal-

108 the proposed algorithm.
 109
 110

2. Related Work

2.1. Weighted Nuclear Norm Minimization

113 As an extension to the nuclear norm minimization
 114 (NNM) model [22], the weighted nuclear norm minimization
 115 (WNNM) model [7] is described as
 116

$$\min_{\mathbf{X}} \|\mathbf{Y} - \mathbf{X}\|_F^2 + \|\mathbf{X}\|_{w,*} \quad (1)$$

117 where $\|\mathbf{X}\|_{w,*} = \sum_i w_i \sigma_i(\mathbf{X})$ is the weighted nuclear
 118 norm of matrix \mathbf{X} , and $w = [w_1, \dots, w_n]^T$, $w_i \geq 0$ is the
 119 weight vector, $\sigma_i(\mathbf{X})$ is the i -th singular value of matrix \mathbf{X} .
 120 According to the Corollary 1 of [23], the problem (1) has
 121 closed-form solution if the weights are non-decreasing
 122

$$\hat{\mathbf{X}} = \mathbf{U} \mathcal{S}_{w/2}(\Sigma) \mathbf{V}^T \quad (2)$$

123 where $\mathbf{Y} = \mathbf{U} \Sigma \mathbf{V}^T$ is the singular value decomposition
 124 of \mathbf{Y} and $\mathcal{S}_\tau(\bullet)$ is the generalized soft-thresholding
 125 operator with weight vector w :
 126

$$\mathcal{S}_{w/2}(\Sigma_{ii}) = \max(\Sigma_{ii} - w_{ii}/2, 0) \quad (3)$$

127 Though having achieved excellent performance on
 128 grayscale image denoising, the WNNM model would generate
 129 false colors or artifacts [14], if being directly extended
 130 to real color image denoising by processing each channel
 131 separately or joint vectors concatenated by multiple channels.
 132 In this paper, for real noisy image denoising, we propose
 133 a multi-channel WNNM model which preserve the power of
 134 WNNM and be able to process the differences among
 135 different channels.
 136

2.2. Real Color Image Denoising

137 During the last decade, several denoising methods are
 138 proposed for real color image denoising [15–17, 19].
 139 Among them, the CBM3D [15] first transform the RGB image
 140 into luminance-chrominance space (e.g., YCbCr) and
 141 then apply the famous BM3D method [2] on each channel
 142 separately with the patches being grouped only in the
 143 luminance channel. In [16], the authors proposed the “Noise
 144 Level Function” to estimate and remove the noise for each
 145 channel in natural images. However, the methods processing
 146 each channel separately would achieve inferior performance
 147 than processing jointly these channels [14]. The methods of [17, 19, 25]
 148 perform real color image denoising by concatenating the patches in R, G, B
 149 channels into joint vectors. However, the concatenation would treat each
 150 channel equally and ignore the different noise properties
 151 among these channels. The method in [18] models the
 152 cross-channel noise in real noisy image as a multivariate
 153 Gaussian and the noise is removed by the Bayesian nonlocal
 154 means filter [26]. The commercial software Neat Image
 155 [27] estimates the noise parameters from a flat region of the
 156

157 given noisy image and filters the noise correspondingly. But
 158 these methods [18, 27] ignore the non-local self similarity
 159 property of natural images [2, 7].
 160

161 In this paper, we introduce a weighting matrix which
 162 add different weights to different channels for color image
 163 denoising. The proposed multi-channel method can effectively
 164 solve the problem of different noise structures among
 165 different channels.
 166

3. Color Image Denoising via Multi-channel Weighted Nuclear Norm Minimization

3.1. The Problem

167 The color image denoising problem is to recover the
 168 clean image $\{\mathbf{x}_c\}$ from its noisy version $\mathbf{y}_c = \mathbf{x}_c + \mathbf{n}_c$,
 169 where $c \in \{r, g, b\}$ is the index of R, G, B channels and
 170 \mathbf{n}_c is the noise in c -th channel. The noise structures in
 171 each channel are different due to the on-board processing
 172 of the in-camera imaging pipeline [13]. Therefore, it is
 173 problematic to directly apply denoising methods to the joint
 174 vectors concatenated by corresponding patches of the R,
 175 G, B channels. To validate this point, in Fig. 1, we show
 176 the clean image “kodim23” taken from the Kodak PhotoCD
 177 dataset, its degraded version generated by adding synthetic
 178 additive white Gaussian noise (AWGN) to each channel of
 179 “kodim23”, and the denoised image by applying WNNM
 180 [7] on the joint vectors concatenated from R, G, B channels
 181 of the degraded image. The standard derivations of AWGN
 182 added to the R, G, B channels are $\sigma_r = 40$, $\sigma_g = 20$,
 183 $\sigma_b = 30$, respectively. The input standard derivation of
 184 the noise for the concatenated WNNM method is set as the
 185 Root Mean Square (RMS) of those in each channel, i.e.,
 186 $\sigma = \sqrt{(\sigma_r^2 + \sigma_g^2 + \sigma_b^2)/3} = 31.1$. From Fig. 1, one can see
 187 that the concatenated WNNM method treating each channel
 188 equally would remain some noise in the R and B channel,
 189 while oversmoothing the G channel of the degraded image.
 190 Hence, if the patches of different channels are treated adaptively
 191 in the concatenated vectors, the degraded color images
 192 would be recovered with better visual qualities.
 193

194 In order to process each channel differently while still
 195 exploiting the joint structures of the color images, in this
 196 paper, we introduce a weighting matrix \mathbf{W} to the concatenated
 197 WNNM method. Assume the matrix \mathbf{Y} containing the
 198 noisy patches in R, G, B channels as $\mathbf{Y} = [\mathbf{Y}_r^T \mathbf{Y}_g^T \mathbf{Y}_b^T]^T$,
 199 the corresponding clean matrix $\mathbf{X} = [\mathbf{X}_r^T \mathbf{X}_g^T \mathbf{X}_b^T]^T$, and
 200 the weights w for the singular values of \mathbf{X} , then the pro-
 201 posed multi-channel WNNM (MC-WNNM) model is
 202

$$\min_{\mathbf{X}} \|\mathbf{W}(\mathbf{Y} - \mathbf{X})\|_F^2 + \|\mathbf{X}\|_{w,*}. \quad (4)$$

203 How to set the weighting matrix \mathbf{W} and how to solve the
 204 proposed model will be introduced in the next sections.
 205

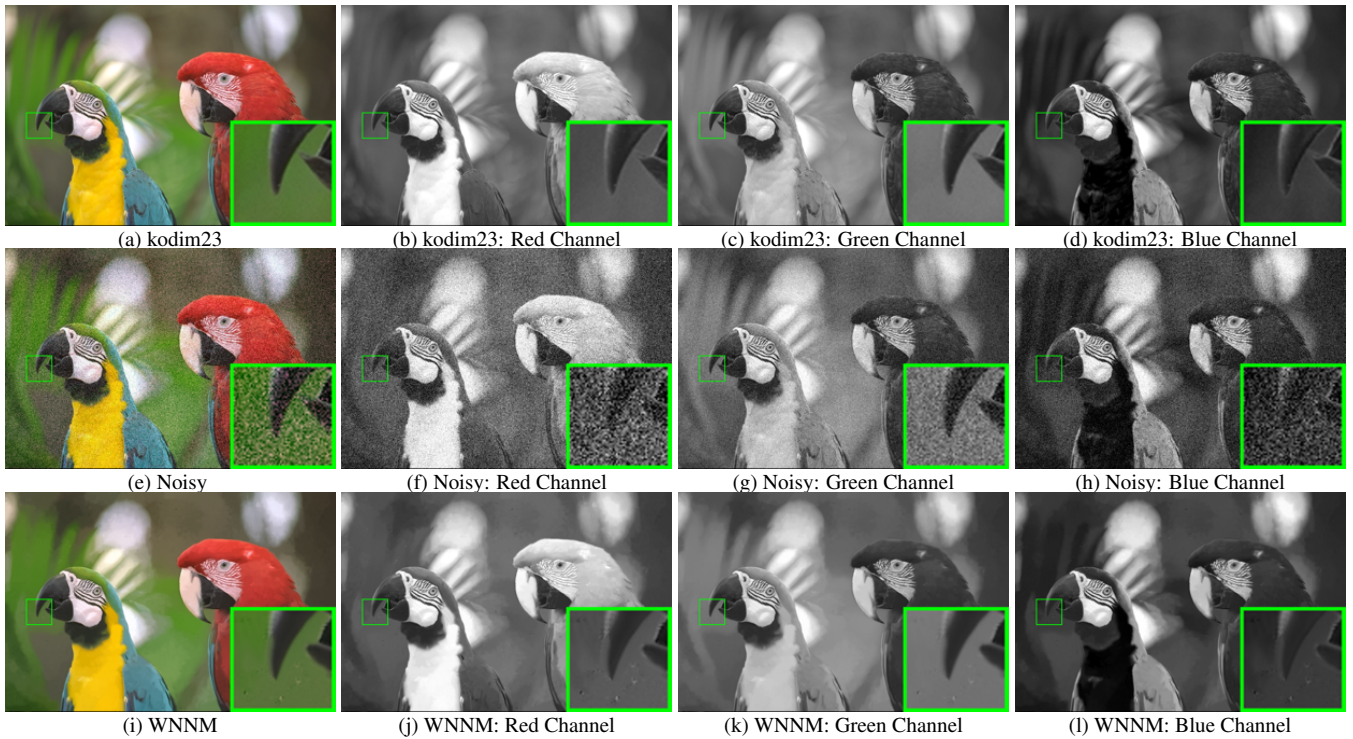


Figure 1. The image “kodim23” of the Kodak PhotoCD dataset, its degraded version, and the image recovered by WNNM. The R, G, B channels are also listed here for image quality comparison.

3.2. The Setting of Weighting Matrix \mathbf{W}

For simplicity, in this paper, we assume the noise are independent among the R, G, B channels and i.i.d. in each channel. Therefore, the weighting matrix \mathbf{W} is diagonal and can be determined under the Bayesian framework:

$$\begin{aligned} \hat{\mathbf{X}} &= \arg \max_{\mathbf{X}} \ln P(\mathbf{X}|\mathbf{Y}, \mathbf{w}) \\ &= \arg \max_{\mathbf{X}} \{\ln P(\mathbf{Y}|\mathbf{X}) + \ln P(\mathbf{X}|\mathbf{w})\}. \end{aligned} \quad (5)$$

The log-likelihood term $\ln P(\mathbf{Y}|\mathbf{X})$ is characterized by the statistics of noise, which is assumed to be channel-wise independent white Gaussian with standard deviations $\{\sigma_r, \sigma_g, \sigma_b\}$

$$P(\mathbf{Y}|\mathbf{X}) = \prod_{c \in \{r, g, b\}} (2\pi\sigma_c^2)^{-\frac{3p^2}{2}} \exp\left(-\frac{1}{2\sigma_c^2} \|\mathbf{Y}_c - \mathbf{X}_c\|_F^2\right). \quad (6)$$

We assume that the matrix \mathbf{X} follows the following distribution

$$P(\mathbf{X}|\mathbf{w}) \propto \exp\left(-\frac{1}{2} \|\mathbf{X}\|_{\mathbf{w},*}\right). \quad (7)$$

Putting (7) and (6) into (5), we have

$$\hat{\mathbf{X}} = \arg \min_{\mathbf{X}} \|\mathbf{W}(\mathbf{Y} - \mathbf{X})\|_F^2 + \|\mathbf{X}\|_{\mathbf{w},*}, \quad (8)$$

where

$$\mathbf{W} = \begin{pmatrix} \sigma_r^{-1} \mathbf{I} & \mathbf{0} & \mathbf{0} \\ \mathbf{0} & \sigma_g^{-1} \mathbf{I} & \mathbf{0} \\ \mathbf{0} & \mathbf{0} & \sigma_b^{-1} \mathbf{I} \end{pmatrix}. \quad (9)$$

where $\mathbf{I} \in \mathbb{R}^{p^2 \times p^2}$ is the identity matrix. Hence, the weighting matrix \mathbf{W} is determined to contribute equal weights for the pixel values in the same channel, while different weights for those in different channels. The experimental (which will be introduced later) results have already demonstrated that this form of weighting matrix have already generated the best denoising performance on synthetic and real noisy images in benchmark datasets.

3.3. The Denoising Algorithm

In this section, with the proposed MC-WNNM model, we propose a denoising algorithm for color images. In our algorithm, given a noisy image \mathbf{y} , each local patch is extracted from it with patch size $p \times p \times 3$ and stretched to a patch vector $\mathbf{y}_j \in \mathbb{R}^{3p^2}$ concatenated by corresponding patches in R, G, B, channels. Then we search the M most similar patches to \mathbf{y}_j (including \mathbf{y}_j itself) by Euclidean distance in a $W \times W$ local region around it. We stack the M similar patches column by column to form a noisy patch matrix $\mathbf{Y}_j = \mathbf{X}_j + \mathbf{N}_j \in \mathbb{R}^{3p^2 \times M}$, where \mathbf{X}_j and \mathbf{N}_j the corresponding clean and noise patch matrices. Then, we can apply the proposed MC-WNNM model to \mathbf{Y}_j to estimate \mathbf{X}_j for color image denoising:

$$\min_{\mathbf{X}_j} \|\mathbf{W}_j(\mathbf{Y}_j - \mathbf{X}_j)\|_F^2 + \|\mathbf{X}_j\|_{\mathbf{w},*}. \quad (10)$$

where \mathbf{W}_j is defined in Eq. (9). Just as [23] did, the weight vector \mathbf{w} is set $w_i^{k+1} = \frac{C}{|\sigma_i(\mathbf{X}_k)| + \epsilon}$ and $\epsilon > 0$ is a small

324
Algorithm 1: Color Image Denoising by MC-WNNM
325 **Input:** Noisy image \mathbf{y} , noise levels $\{\sigma_r, \sigma_g, \sigma_b\}$;
326 **Initialization:** $\hat{\mathbf{x}}^{(0)} = \mathbf{y}, \mathbf{y}^{(0)} = \mathbf{y}$;
327 **for** $k = 1 : K_1$ **do**
328 1. Set $\mathbf{y}^{(k)} = \hat{\mathbf{x}}^{(k-1)}$;
329 2. Extracte local patches $\{\mathbf{y}_j\}_{j=1}^N$ from $\mathbf{y}^{(k)}$;
330 **for** each patch \mathbf{y}_j **do**
331 3. Search non-local similar patches \mathbf{Y}_j ;
332 4. Applying the MC-WNNM model (10) to \mathbf{Y}_j and
333 obtain the estimated \mathbf{X}_j ;
334 **end for**
335 5. Aggregate $\{\mathbf{X}_j\}_{j=1}^N$ to form the image $\hat{\mathbf{x}}^{(k)}$;
336 **end for**
337 **Output:** Denoised image $\hat{\mathbf{x}}^{K_1}$.

340 number to avoid zero numerator. Note that when $\sigma_r = \sigma_g =$
341 σ_b , the multi-channel WNNM model will be reduced to the
342 concatenated WNNM model as a special case.

343 The multi-channel WNNM is applied to the noisy patch
344 matrix \mathbf{Y}_j of each local patch \mathbf{y}_j in the noisy image \mathbf{y} . And
345 then all the patches are aggregated together to form the final
346 recovered image $\hat{\mathbf{y}}$. To obtain better denoising results,
347 we perform the above denoising procedure for several (K_1)
348 iterations. The proposed MC-WNNM denoising algorithm
349 for color images is summarized in Algorithm 1.

350 3.4. Optimization

351 The proposed MC-WNNM model could not be solved
352 in an analytical form while the original WNNM model
353 [23] could. In the WNNM model, when the weights on
354 singular values are non-descending, the weighted nuclear
355 norm proximal operator [23] can have global optimum with
356 closed-form solution. However, such property is not valid
357 for the multi-channel WNNM model. The reason is that the
358 weighting matrix \mathbf{W} is added to the rows of matrix \mathbf{X} instead
359 of its singular values. Besides, the elements in \mathbf{W} is
360 not in a non-descending order with respect to the singular
361 value of \mathbf{X} . This makes the proposed model more difficult
362 to solve when compared to the original WNNM model.

363 By introducing an augmented variable \mathbf{Z} , the MC-
364 WNNM model is reformulated as a linear equality-
365 constrained problem with two variables \mathbf{X} and \mathbf{Z} :

$$366 \min_{\mathbf{X}, \mathbf{Z}} \|\mathbf{W}(\mathbf{Y} - \mathbf{X})\|_F^2 + \|\mathbf{Z}\|_{w,*} \quad \text{s.t. } \mathbf{X} = \mathbf{Z}. \quad (11)$$

370 Since the objective function is separable across the two variables,
371 the problem (11) can be solved under alternating direction
372 method of multipliers (ADMM) framework. We can
373 derive its augmented Lagrangian function:
374

$$375 \mathcal{L}(\mathbf{X}, \mathbf{Z}, \mathbf{A}, \rho) = \|\mathbf{W}(\mathbf{Y} - \mathbf{X})\|_F^2 + \|\mathbf{Z}\|_{w,*} \\ 376 \quad + \langle \mathbf{A}, \mathbf{X} - \mathbf{Z} \rangle + \frac{\rho}{2} \|\mathbf{X} - \mathbf{Z}\|_F^2 \quad (12)$$

377 where \mathbf{A} is the augmented Lagrangian multiplier and $\rho > 0$
378 is the penalty parameter. We initialize the matrix variables
379 \mathbf{X}_0 , \mathbf{Z}_0 , and \mathbf{A}_0 to be zero matrix of suitable size. By tak-
380 ing derivative of the Lagrangian function \mathcal{L} with respect to
381 the variables \mathbf{X} and \mathbf{Z} and setting the derivative function to
382 be zero, we can alternatively update the ADMM algorithm
383 iteratively as follows:

384 (1) **Update \mathbf{X} while fixing \mathbf{Z} and \mathbf{A} :**

$$385 \mathbf{X}_{k+1} = \arg \min_{\mathbf{X}} \|\mathbf{W}(\mathbf{Y} - \mathbf{X})\|_F^2 + \frac{\rho_k}{2} \|\mathbf{X} - \mathbf{Z}_k + \rho_k^{-1} \mathbf{A}_k\|_F^2 \quad (13)$$

386 This is a least squares regression problem with closed-form
387 solution:

$$388 \mathbf{X}_{k+1} = (\mathbf{W}^\top \mathbf{W} + \frac{\rho_k}{2} \mathbf{I})^{-1} (\mathbf{W}^\top \mathbf{W} \mathbf{Y} + \frac{\rho_k}{2} \mathbf{Z}_k - \frac{1}{2} \mathbf{A}_k) \quad (14)$$

389 (2) **Update \mathbf{Z} while fixing \mathbf{X} and \mathbf{A} :**

$$390 \mathbf{Z}_{k+1} = \arg \min_{\mathbf{Z}} \frac{\rho_k}{2} \|\mathbf{Z} - (\mathbf{X}_{k+1} + \rho_k^{-1} \mathbf{A}_k)\|_F^2 + \|\mathbf{Z}\|_{w,*} \quad (15)$$

391 According to the Theorem 1 in [23], given the $\mathbf{X}_{k+1} +$
392 $\rho_k^{-1} \mathbf{A}_k = \mathbf{U}_k \Sigma_k \mathbf{V}_k^\top$ be the SVD of $\mathbf{X}_{k+1} + \rho_k^{-1} \mathbf{A}_k$,
393 where $\Sigma_k = \begin{pmatrix} \text{diag}(\sigma_1, \sigma_2, \dots, \sigma_n) \\ \mathbf{0} \end{pmatrix} \in \mathbb{R}^{m \times n}$, then the
394 global optimum of the above problem is $\hat{\mathbf{Z}} = \mathbf{U}_k \hat{\Sigma}_k \mathbf{V}_k^\top$,
395 where $\hat{\Sigma}_k = \begin{pmatrix} \text{diag}(\hat{\sigma}_1, \hat{\sigma}_2, \dots, \hat{\sigma}_n) \\ \mathbf{0} \end{pmatrix} \in \mathbb{R}^{m \times n}$ and
396 $(\hat{\sigma}_1, \hat{\sigma}_2, \dots, \hat{\sigma}_n)$ is the solution to the following convex optimi-
397 zation problem:

$$398 \min_{\hat{\sigma}_1, \hat{\sigma}_2, \dots, \hat{\sigma}_n} \sum_{i=1}^n (\sigma_i - \hat{\sigma}_i)^2 + \frac{2w_i}{\rho_k} \hat{\sigma}_i \quad (16)$$

s.t. $\hat{\sigma}_1 \geq \hat{\sigma}_2 \geq \dots \geq \hat{\sigma}_n \geq 0$.

400 According to the Remark 1 in [23], the problem above has
401 closed-form solution

$$402 \hat{\sigma}_i = \begin{cases} 0 & \text{if } c_2 < 0 \\ \frac{c_1 + \sqrt{c_2}}{2} & \text{if } c_2 \geq 0 \end{cases} \quad (17)$$

403 where $c_1 = \sigma_i - \epsilon$, $c_2 = (\sigma_i - \epsilon)^2 - \frac{8C}{\rho_k}$ and C is set as
404 $\sqrt{2n}$ by experience in image denoising.

405 (3) **Update \mathbf{A} while fixing \mathbf{X} and \mathbf{Z} :**

$$406 \mathbf{A}_{k+1} = \mathbf{A}_k + \rho_k (\mathbf{X}_{k+1} - \mathbf{Z}_{k+1}) \quad (18)$$

407 (4) **Update ρ_k :** $\rho_{k+1} = \mu * \rho_k$, where $\mu > 1$.

408 The above alternative updating steps are repeated until
409 the convergence condition is satisfied or the number of
410 iterations exceeds a preset maximum number, e.g., K_2 .
411 The convergence condition of the ADMM algorithm is:
412 $\|\mathbf{X}_{k+1} - \mathbf{Z}_{k+1}\|_F \leq \text{Tol}$, $\|\mathbf{X}_{k+1} - \mathbf{X}_k\|_F \leq \text{Tol}$, and
413 $\|\mathbf{Z}_{k+1} - \mathbf{Z}_k\|_F \leq \text{Tol}$ are simultaneously satisfied, where

432	Algorithm 2: Solve MC-WNNM via ADMM	486
433	Input: Matrices \mathbf{Y} and \mathbf{W} , $\mu > 1$, $\text{Tol} > 0$;	487
434	Initialization: $\mathbf{X}_0 = \mathbf{Z}_0 = \mathbf{A}_0 = \mathbf{0}$, $\rho_0 > 0$, $\mathbf{T} = \text{False}$,	488
435	$k = 0$;	489
436	While ($\mathbf{T} == \text{false}$) do	490
437	1. Update \mathbf{X}_{k+1} as	491
438	$\mathbf{X}_{k+1} = (\mathbf{W}^\top \mathbf{W} + \frac{\rho_k}{2} \mathbf{I})^{-1} (\mathbf{W}^\top \mathbf{W} \mathbf{Y} + \frac{\rho_k}{2} \mathbf{Z}_k - \frac{1}{2} \mathbf{A}_k)$	492
439	2. Update \mathbf{Z}_{k+1} by solving the problem	493
440	$\min_{\mathbf{Z}} \frac{\rho_k}{2} \ \mathbf{Z}\ _F^2 + \ \mathbf{Z}\ _{w,*}$	494
441	3. Update \mathbf{A}_{k+1} as $\mathbf{A}_{k+1} = \mathbf{A}_k + \rho_k (\mathbf{X}_{k+1} - \mathbf{Z}_{k+1})$	495
442	4. Update $\rho_{k+1} = \mu * \rho_k$;	496
443	5. $k \leftarrow k + 1$;	497
444	if (Convergence conditions are satisfied) or ($k \geq K_2$)	498
445	5. $\mathbf{T} \leftarrow \text{True}$	499
446	end if	500
447	end while	501
448	Output: Matrices \mathbf{X} and \mathbf{Z} .	502

Tol > 0 is a small tolerance. We summarize the optimization steps in Algorithm 2. The convergence analysis of the proposed Algorithm 2 is given in Theorem 1. Note that since the weighted nuclear norm is non-convex in general, we employ an unbounded sequence of $\{\rho_k\}$ here to make sure that the Algorithm 2 is convergent.

Theorem 1. Assume the weights in w are in a non-descending order, the sequence $\{\mathbf{X}_k\}$, $\{\mathbf{Z}_k\}$, and $\{\mathbf{A}_k\}$ generated in Algorithm 1 satisfy:

$$(a) \lim_{k \rightarrow \infty} \|\mathbf{X}_{k+1} - \mathbf{Z}_{k+1}\|_F = 0; \quad (19)$$

$$(b) \lim_{k \rightarrow \infty} \|\mathbf{X}_{k+1} - \mathbf{X}_k\|_F = 0; \quad (20)$$

$$(c) \lim_{k \rightarrow \infty} \|\mathbf{Z}_{k+1} - \mathbf{Z}_k\|_F = 0. \quad (21)$$

Proof. We give proof sketch here and detailed proof of this theorem can be found in supplementary files. We can first proof that the sequence $\{\mathbf{A}_k\}$ generated by Algorithm 3.4 is upper bounded. Since $\{\rho_k\}$ is unbounded, that is $\lim_{k \rightarrow \infty} \rho_k = +\infty$, we can proof that the sequence of Lagrangian function $\{\mathcal{L}(\mathbf{X}_{k+1}, \mathbf{Z}_{k+1}, \mathbf{A}_k, \rho_k)\}$ is also upper bounded. Hence, both $\{\mathbf{W}(\mathbf{Y} - \mathbf{X}_k)\}$ and $\{\mathbf{Z}_k\}$ are upper bounded. According to Eq. (18), we can proof that $\lim_{k \rightarrow \infty} \|\mathbf{X}_{k+1} - \mathbf{Z}_{k+1}\|_F = \lim_{k \rightarrow \infty} \rho_k^{-1} \|\mathbf{A}_{k+1} - \mathbf{A}_k\|_F = 0$, and (a) is proofed. Then we can proof that $\lim_{k \rightarrow \infty} \|\mathbf{X}_{k+1} - \mathbf{X}_k\|_F \leq \lim_{k \rightarrow \infty} \|(\mathbf{W}^\top \mathbf{W} + \frac{\rho_k}{2} \mathbf{I})^{-1} (\mathbf{W}^\top \mathbf{W} \mathbf{Y} - \mathbf{W}^\top \mathbf{W} \mathbf{Z}_k - \frac{1}{2} \mathbf{A}_k)\|_F + \rho_k^{-1} \|\mathbf{A}_k - \mathbf{A}_{k-1}\|_F = 0$ and hence (b) is proofed. Then (c) can be proofed by checking that $\lim_{k \rightarrow \infty} \|\mathbf{Z}_{k+1} - \mathbf{Z}_k\|_F \leq \lim_{k \rightarrow \infty} \|\Sigma_{k-1} - S_{w/\rho_{k-1}}(\Sigma_{k-1})\|_F + \|\mathbf{X}_{k+1} - \mathbf{X}_k\|_F + \rho_k^{-1} \|\mathbf{A}_{k-1} + \mathbf{A}_{k+1} - \mathbf{A}_k\|_F = 0$, where $\mathbf{U}_{k-1} \Sigma_{k-1} \mathbf{V}_{k-1}^\top$ is the SVD of the matrix $\mathbf{X}_k + \rho_{k-1} \mathbf{A}_{k-1}$. \square

4. Experiments

We evaluate the proposed MC-WNNM method on synthetic and real color image denoising. We compare the proposed method with other state-of-the-art denoising methods including CBM3D [15], MLP [10], WNNM [7], TNRD [12], “Noise Clinic” (NC) [17, 25], and the commercial software Neat Image (NI) [27].

4.1. Implementation Details

In synthetic experiments, the noise levels in R, G, B channels are assumed to be known as $\sigma_r, \sigma_g, \sigma_b$. In the real cases, the noise levels in R, G, B channels can be estimated via noise estimation methods [28, 29]. In this paper, we employ the method of [29] for its state-of-the-art performance. For the CBM3D method [15], the input noise levels are the Root Mean Square (RMS) as

$$\sigma = \sqrt{(\sigma_r^2 + \sigma_g^2 + \sigma_b^2)/3}. \quad (22)$$

For the methods of MLP [10] and TNRD [12], we retrain the models on grayscale images following their corresponding strategies at different noise levels from $\sigma = 5$ to $\sigma = 75$ with gap of 5. The denoising on color images is performed by processing separately each channel with the model trained at the same (or nearest) noise levels. NC [17, 25] is a blind image denoising method, so we just submit the noisy images (synthetic or real) to [25] and perform denoising using the default parameters. NI [27] is a commercial software suitable for real image denoising, while the code of CC [18] is not released (but its results on the 15 real noisy images in [18] are available by requesting the authors). Hence, we only compare with CC and NI in real image denoising experiments, and do not compare with them in synthetic experiments.

In order to take fully comparison with the original WNNM method [23], we extended the WNNM method [23] for color image denoising in three directions: 1) we apply the WNNM method [23] on each channel separately with corresponding noise levels $\sigma_r, \sigma_g, \sigma_b$. We call this method “WNNM0”; 2) we perform denoising on the joint vectors concatenated by corresponding patches in the R, G, B channels, where the input noise level σ is computed by RMS (Eq. (22)). We call this method “WNNM1”; 3) we set the weighting matrix \mathbf{W} in the proposed MC-WNNM model as $\mathbf{W} = \sigma^{-1} \mathbf{I}$. For fair comparison, we tune all these methods set the same parameters for “WNNM2” and the proposed MC-WNNM methods while achieving the best performance of “WNNM2”. For fair comparison, we tune the methods of “WNNM0”, “WNNM1”, “WNNM2”, and the proposed MC-WNNM to achieve corresponding best denoising performance (i.e., highest average PSNR results).

4.2. Experiments on Synthetic Noisy Images

In this section, we compare the proposed MC-WNNM method with other competing method [10, 12, 15, 17,



Figure 2. The 24 high quality color images from the Kodak PhotoCD Dataset.

[27] as well as the three extensions of WNNM [23] on the 24 high quality color images from the Kodak PhotoCD Dataset (<http://r0k.us/graphics/kodak/>), which are shown in Fig. 2. The noisy images are generated by adding additive white Gaussian noise (AWGN) with known standard derivations $\sigma_r, \sigma_g, \sigma_b$ for the R, G, B channels, respectively. In this paper, the noise levels we add to each channel of the 24 color images are $\sigma_r = 40, \sigma_g = 20, \sigma_b = 30$, respectively. More experiments can be found in the supplementary files. For the methods of “WNNM2” and MC-WNNM, we set the patch size as $p = 6$, the number of non-local similar patches as $M = 70$, the window size for searching similar patches as $W = 20$, the updating parameter $\mu = 1.001$, the number of iterations in Algorithm 1 as $K_1 = 8$, the number of iterations in Algorithm 2 as $K_2 = 10$. For “WNNM2”, the initial penalty parameter is set as $\rho_0 = 10$, while for the proposed MC-WNNM model, the penalty parameter is set as $\rho_0 = 3$.

The PSNR results are listed in Table 1 of the compared methods including CBM3D [15], MLP [10], TNRD [12], NI [27], NC [17, 25], “WNNM0” [23], “WNNM1”, “WNNM2” and the proposed MC-WNNM methods. The best PSNR results are highlighted in bold. One can see that on all the 24 images, our method achieves the highest PSNR values over the competing methods. On average PSNR, our proposed method achieves 0.48dB improvements over the “WNNM0” method and outperforms the “WNNM2” by 1.09dB. Fig. 3 shows a scene denoised by the compared methods. We can see that CBM3D and NC would remain noise while MLP and TNRD would generate artifacts. The methods of “WNNM0”, “WNNM1”, “WNNM2” would over-smooth much the image. By using the proposed MC-WNNM model, our method preserves the structures (e.g., edges and textures) better across the R, G, B channels and generate less artifacts than other denoising methods, leading to visually pleasant outputs. More visual comparisons can be found in the supplementary files.

4.3. Experiments on Real Noisy Images

In this section, we compare the proposed MC-WNNM method with other competing methods on the 15 real noisy images (Fig. 4). We do not compare with the “WNNM0” method due to limited space and its inferior performance. The noisy images were collected under controlled indoor environment. Each scene was shot 500 times under the same camera and camera setting. The mean image of the 500 shots is roughly taken as the “ground truth”, with which the PSNR can be computed. Since the image size is very large (about 7000×5000) and the 11 scenes share repetitive contents, the authors of [18] cropped 15 smaller images (of size 512×512) to perform experiments. For each real noisy image, the noise levels in R, G, B channels are estimated by [29]. Since the noise levels are small in real noisy images, for the method of MLP [10] and TNRD [12], we apply the trained models of corresponding methods and choose the best denoising results (highest average PSNR values). Both methods achieves best results when setting the noise levels of the trained models from $\sigma = 10$.

We perform quantitative comparison on the 15 cropped images used in [18]. The PSNR results are listed in Table 2 of the compared methods including CBM3D [15], MLP [10], TNRD [12], NC [17, 25], NI [27], CC [18] (copied from [18]), “WNNM1”, “WNNM2”, and the proposed MC-WNNM method. The highest PSNR results are highlighted in bold. On average PSNR, the proposed MC-WNNM method achieves 0.44dB improvements over the “WNNM1” method and outperforms the state-of-the-art denoising method CC [18] by 0.83dB. On 10 out of the whole 15 images, the proposed MC-WNNM method achieves the highest PSNR values. Both CC and “WNNM1” achieves highest PSNR results on 2 of 15 images. It should be noted that in the CC method, a specific model is trained for each camera and camera setting, while our method uses the same model for all images. Fig. 5 shows the denoised images of a scene captured by Canon 5D Mark 3 at ISO = 3200. We can see that CBM3D, NC, NI and CC would either remain noise or generate artifacts, while TNRD over-smooth much the image. By using the proposed MC-WNNM model achieves better visual quality results than other methods. More visual comparisons can be found in the supplementary files.

5. Conclusion and Future Work

The real noisy images have different noise structures among the R, G, B channels due to the preprocessing steps of the in-camera imaging pipelines in CCD or CMOS sensors. This makes the real image denoising problem much more complex than grayscale image denoising. In this paper, we proposed a novel multi-channel (MC) model for real color image denoising. By introducing a weighting matrix to the concatenated weighted nuclear norm minimiza-

540		594
541		595
542		596
543		597
544		598
545		599
546		600
547		601
548		602
549		603
550		604
551		605
552		606
553		607
554		608
555		609
556		610
557		611
558		612
559		613
560		614
561		615
562		616
563		617
564		618
565		619
566		620
567		621
568		622
569		623
570		624
571		625
572		626
573		627
574		628
575		629
576		630
577		631
578		632
579		633
580		634
581		635
582		636
583		637
584		638
585		639
586		640
587		641
588		642
589		643
590		644
591		645
592		646
593		647

648

649

650

651

652

653

654

655

656

657

658

659

660

661

662

663

664

665

666

667

668

669

670

671

672

673

674

675

676

677

678

679

680

681

682

683

684

685

686

687

688

689

690

691

692

693

694

695

696

697

698

699

700

701

702

703

704

705

706

707

708

709

710

711

712

713

714

715

716

717

718

719

720

721

722

723

724

725

726

727

728

729

730

731

732

733

734

735

736

737

738

739

740

741

742

743

744

745

746

747

748

749

750

751

752

753

754

755

Table 1. PSNR(dB) results of different denoising algorithms on 24 natural images.

Image#	CBM3D	MLP	TNRD	NI	NC	WNNM0	WNNM1	WNNM2	MC-WNNM
1	25.24	25.70	25.74	23.85	24.90	26.01	25.95	25.58	26.66
2	28.27	30.12	30.21	25.90	25.87	30.08	30.11	29.80	30.20
3	28.81	31.19	31.49	26.00	28.58	31.58	31.61	31.20	32.25
4	27.95	29.88	29.86	25.82	25.67	30.13	30.16	29.84	30.49
5	25.03	26.00	26.18	24.38	25.15	26.44	26.39	25.32	26.82
6	26.24	26.84	26.90	24.65	24.74	27.39	27.30	26.88	27.98
7	27.88	30.28	30.40	25.63	27.69	30.47	30.54	29.70	30.98
8	25.05	25.59	25.83	24.02	25.30	26.71	26.75	25.26	26.90
9	28.44	30.75	30.81	25.94	27.44	30.86	30.92	30.29	31.49
10	28.27	30.38	30.57	25.87	28.42	30.65	30.68	29.95	31.26
11	26.95	28.00	28.14	25.32	24.67	28.19	28.16	27.61	28.63
12	28.76	30.87	31.05	26.01	28.37	30.97	31.06	30.58	31.48
13	23.76	23.95	23.99	23.53	22.76	24.27	24.15	23.52	24.89
14	26.02	26.97	27.11	24.94	25.68	27.20	27.15	26.55	27.57
15	28.38	30.15	30.44	26.06	28.21	30.52	30.60	30.13	30.81
16	27.75	28.82	28.87	25.69	26.66	29.27	29.21	29.02	29.96
17	27.90	29.57	29.80	25.85	28.32	29.78	29.79	29.16	30.40
18	25.77	26.40	26.41	24.74	25.70	26.63	26.56	26.01	27.22
19	27.30	28.67	28.81	25.40	26.52	29.19	29.22	28.67	29.57
20	28.96	30.40	30.76	24.95	25.90	30.79	30.83	29.97	31.07
21	26.54	27.53	27.60	25.06	26.48	27.80	27.75	27.12	28.34
22	27.05	28.17	28.27	25.36	26.60	28.21	28.16	27.81	28.64
23	29.14	32.31	32.51	26.13	23.24	31.89	31.97	31.21	32.34
24	25.75	26.41	26.53	24.55	25.73	27.10	27.03	26.18	27.59
Average	27.13	28.54	28.68	25.24	26.19	28.84	28.83	28.22	29.31



Figure 3. Denoised images of different methods on the image “kodim07” degraded by noise with different levels on different channels. The images are better to be zoomed in on screen.

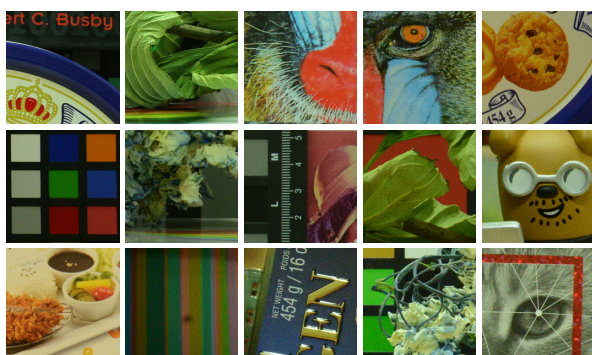


Figure 4. The 15 cropped real noisy images used in [18].

tion (WNNM) model, the proposed MC-WNNM model can process adaptively the different noise structures in each of the R, G, B channels and exploit the non-local self similarity property of natural images. Though no longer hav-

ing closed-form solution, we successfully solved the MC-WNNM model via an ADMM algorithm by reformulating the MC-WNNM model as a linear equality-constrained problem with two separable variables. We also studied the convergence property of the ADMM algorithm. Extensive experiments on synthetic and real-world noisy images demonstrate that, the proposed MC-WNNM model outperforms the other competing denoising methods on both synthetic color noisy images as well as real-world noisy images. The introduce of the weighting matrix can boost the performance of traditional models on new applications. We believe that this work can be extended in at least two directions. Firstly, the weighting matrix beyond the diagonal form, such as correlation form [30], may bring better performance on color image denoising. Secondly, the proposed MC-WNNM model can be further extended to deal with hy-

Table 2. PSNR(dB) results of different methods on 15 cropped real noisy images used in [18].

Camera Settings	CBM3D	MLP	TNRD	NI	NC	CC	WNNM1	WNNM2	MC-WNNM
Canon 5D Mark III ISO = 3200	39.76 36.40 36.37	39.00 36.34 36.33	39.51 36.47 36.45	35.68 34.03 32.63	36.20 34.35 33.10	38.37 35.37 34.91	39.74 35.12 33.14	39.98 36.65 34.63	41.13 37.28 36.52
Nikon D600 ISO = 3200	34.18 35.07 37.13	34.70 36.20 39.33	34.79 36.37 39.49	31.78 35.16 39.98	32.28 35.34 40.51	34.98 35.95 41.15	35.08 36.42 40.78	35.08 36.84 39.24	35.53 37.02 39.56
Nikon D800 ISO = 1600	36.81 37.76 37.51	37.95 40.23 37.94	38.11 40.52 38.17	34.84 38.42 35.79	35.09 38.65 35.85	37.99 40.36 38.30	38.28 41.24 38.04	38.61 40.81 38.96	39.26 41.43 39.55
Nikon D800 ISO = 3200	35.05 34.07 34.42	37.55 35.91 38.15	37.69 35.90 38.21	38.36 35.53 40.05	38.56 35.76 40.59	39.01 36.75 39.06	39.93 37.32 41.52	37.97 37.30 38.68	38.91 37.41 39.39
Nikon D800 ISO = 6400	31.13 31.22 30.97	32.69 32.33 32.29	32.81 32.33 32.29	34.08 32.13 31.52	34.25 32.38 31.76	34.61 33.21 33.22	35.20 33.61 33.62	34.57 33.43 34.02	34.80 33.95 33.94
Average	35.19	36.46	36.61	35.33	35.65	36.88	37.27	37.12	37.71

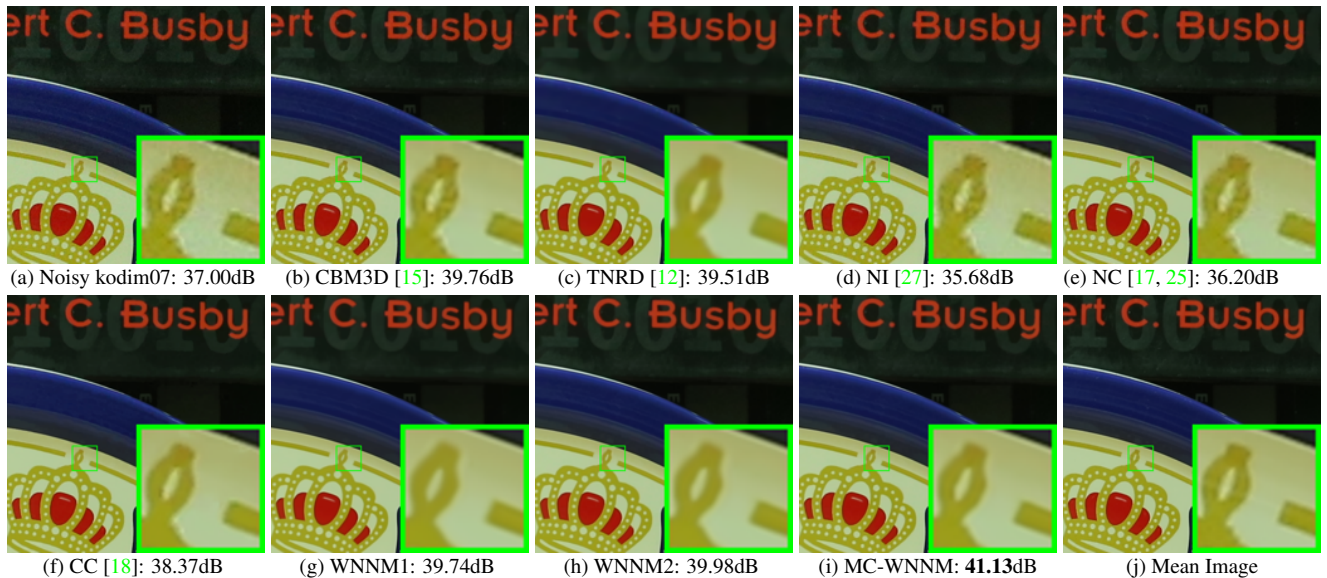


Figure 5. Denoised images of a region cropped from the real noisy image “Canon 5D Mark 3 ISO 3200 1” [18] by different methods. The images are better to be zoomed in on screen.

perspectral images, which contain much more channels than color images.

References

- [1] A. Buades, B. Coll, and J. M. Morel. A non-local algorithm for image denoising. *IEEE Conference on Computer Vision and Pattern Recognition (CVPR)*, pages 60–65, 2005. [1](#)
- [2] K. Dabov, A. Foi, V. Katkovnik, and K. Egiazarian. Image denoising by sparse 3-D transform-domain collabora-
- tive filtering. *IEEE Transactions on Image Processing*, 16(8):2080–2095, 2007. [1, 2](#)
- [3] M. Elad and M. Aharon. Image denoising via sparse and redundant representations over learned dictionaries. *IEEE Transactions on Image Processing*, 15(12):3736–3745, 2006.
- [4] J. Mairal, F. Bach, J. Ponce, G. Sapiro, and A. Zisserman. Non-local sparse models for image restoration. *IEEE International Conference on Computer Vision (ICCV)*, pages 2272–2279, 2009.

- 864 [5] W. Dong, L. Zhang, G. Shi, and X. Li. Nonlocally central- 918
865 ized sparse representation for image restoration. *IEEE Trans- 919
866 actions on Image Processing*, 22(4):1620–1630, 2013. 920
867
868 [6] J. Xu, L. Zhang, W. Zuo, D. Zhang, and X. Feng. Patch 921
869 group based nonlocal self-similarity prior learning for image 922
870 denoising. *IEEE International Conference on Computer Vi- 923
871 sion (ICCV)*, pages 244–252, 2015. 924
872
873 [7] S. Gu, L. Zhang, W. Zuo, and X. Feng. Weighted nu- 925
874 clear norm minimization with application to image denois- 926
875 ing. *IEEE Conference on Computer Vision and Pattern 927
876 Recognition (CVPR)*, pages 2862–2869, 2014. 1, 2, 5
877
878 [8] S. Roth and M. J. Black. Fields of experts. *International 928
879 Journal of Computer Vision*, 82(2):205–229, 2009. 1
880
881 [9] D. Zoran and Y. Weiss. From learning models of natural 929
882 image patches to whole image restoration. *IEEE Interna- 930
883 tional Conference on Computer Vision (ICCV)*, pages 479– 931
884 486, 2011. 932
885
886 [10] H. C. Burger, C. J. Schuler, and S. Harmeling. Image 933
887 denoising: Can plain neural networks compete with BM3D? 934
888 *IEEE Conference on Computer Vision and Pattern Recog- 935
889 nition (CVPR)*, pages 2392–2399, 2012. 5, 6, 7
890
891 [11] U. Schmidt and S. Roth. Shrinkage fields for effective 936
892 image restoration. *IEEE Conference on Computer Vision and 937
893 Pattern Recognition (CVPR)*, pages 2774–2781, June 2014. 938
894
895 [12] Y. Chen, W. Yu, and T. Pock. On learning optimized 939
896 reaction diffusion processes for effective image restoration. 940
897 *IEEE Conference on Computer Vision and Pattern Recog- 941
898 nition (CVPR)*, pages 5261–5269, 2015. 1, 5, 6, 7, 8
899
900 [13] H. C. Karaimer and M. S. Brown. A software platform for 942
901 manipulating the camera imaging pipeline. *European Con- 943
902 ference on Computer Vision (ECCV)*, October 2016. 1, 2
903
904 [14] Julien Mairal, Michael Elad, and Guillermo Sapiro. Sparse 944
905 representation for color image restoration. *IEEE Transac- 945
906 tions on Image Processing*, 17(1):53–69, 2008. 1, 2
907
908 [15] K. Dabov, A. Foi, V. Katkovnik, and K. Egiazarian. Color 946
909 image denoising via sparse 3D collaborative filtering with 947
910 grouping constraint in luminance-chrominance space. *IEEE 948
911 International Conference on Image Processing (ICIP)*, pages 949
912 313–316, 2007. 1, 2, 5, 6, 7, 8
913
914 [16] C. Liu, R. Szeliski, S. Bing Kang, C. L. Zitnick, and W. T. 950
915 Freeman. Automatic estimation and removal of noise from 951
916 a single image. *IEEE Transactions on Pattern Analysis and 952
917 Machine Intelligence*, 30(2):299–314, 2008. 1, 2
918
919 [17] M. Lebrun, M. Colom, and J.-M. Morel. Multiscale image 953
920 blind denoising. *IEEE Transactions on Image Processing*, 954
921 24(10):3149–3161, 2015. 2, 5, 6, 7, 8
922
923 [18] S. Nam, Y. Hwang, Y. Matsushita, and S. J. Kim. A holistic 955
924 approach to cross-channel image noise modeling and its ap- 956
925 plication to image denoising. *IEEE Conference on Computer 957
926 Vision*, 2015. 958
927
928 [19] F. Zhu, G. Chen, and P.-A. Heng. From noise modeling to 959
929 blind image denoising. *IEEE Conference on Computer Vi- 960
930 sion and Pattern Recognition (CVPR)*, June 2016. 1, 2
931
932 [20] S. Boyd, N. Parikh, E. Chu, B. Peleato, and J. Eckstein. Dis- 961
933 tributed optimization and statistical learning via the alternat- 962
934 ing direction method of multipliers. *Found. Trends Mach. 963
935 Learn.*, 3(1):1–122, January 2011. 1
936
937 [21] C. Lu, C. Zhu, C. Xu, S. Yan, and Z. Lin. Generalized sin- 938
939 gular value thresholding. *AAAI*, 2015. 1
940
941 [22] J. Cai, E. J. Candès, and Z. Shen. A singular value thresh- 942
942 olding algorithm for matrix completion. *SIAM Journal on 943
943 Optimization*, 20(4):1956–1982, 2010. 2
944
945 [23] S. Gu, Q. Xie, D. Meng, W. Zuo, X. Feng, and L. Zhang. 946
946 Weighted nuclear norm minimization and its applications to 947
947 low level vision. *International Journal of Computer Vision*, 948
948 pages 1–26, 2016. 2, 3, 4, 5, 6
949
950 [24] C. Eckart and G. Young. The approximation of one matrix by 951
951 another of lower rank. *Psychometrika*, 1(3):211–218, 1936. 2
952
953 [25] M. Lebrun, M. Colom, and J. M. Morel. The noise clinic: 954
954 a blind image denoising algorithm. [http://www.ipol. 955
955 im/pub/art/2015/125/](http://www.ipol.im/pub/art/2015/125/). Accessed 01 28, 2015. 2, 5, 6, 7, 8
956
957 [26] C. Kervrann, J. Boulanger, and P. Coupé. Bayesian non- 958
958 local means filter, image redundancy and adaptive dictionaries 959
959 for noise removal. *International Conference on Scale 960
960 Space and Variational Methods in Computer Vision*, pages 961
961 520–532, 2007. 2
962
963 [27] Neatlab ABSsoft. Neat Image. [https://ni. 964
964 neatvideo.com/home](https://ni.neatvideo.com/home). 2, 5, 6, 8
965
966 [28] X. Liu, M. Tanaka, and M. Okutomi. Single-image noise 967
967 level estimation for blind denoising. *IEEE Transactions on 968
968 Image Processing*, 22(12):5226–5237, 2013. 5
969
970 [29] G. Chen, F. Zhu, and A. H. Pheng. An efficient statistical 971
971 method for image noise level estimation. *IEEE Interna- 972
972 tional Conference on Computer Vision (ICCV)*, December 2015. 5, 6
973
974 [30] N. J. Higham. Computing the nearest correlation matrixa 975
975 problem from finance. *IMA Journal of Numerical Analysis*, 976
976 22(3):329, 2002. 7
977